ISSN 0027-1349, Moscow University Physics Bulletin, 2024, Vol. 79, Suppl. 2, pp. S724–S730. © Allerton Press, Inc., 2024.

Evaluating EAS Directions from TAIGA HiSCORE Data Using Fully Connected Neural Networks

A. P. Kryukov[1*], S. P. Polyakov[1], Yu. Yu. Dubenskaya[1], E. O. Gres[1,2], E. B. Postnikov[1], P. A. Volchugov[1], and D. P. Zhurov[1,2]**

[1]*Skobeltsyn Institute of Nuclear Physics, Lomonosov Moscow State University, Moscow, Russia*

[2]*Research Institute of Applied Physics, Irkutsk State University, Irkutsk, 664003 Russia*

Received October 1, 2024; revised October 10, 2024; accepted October 20, 2024

Abstract—The TAIGA-HiSCORE setup is a wide-angle Cherenkov detector array for recording extensive air showers (EASs). The array comprises over 120 stations located in the Tunka Valley near Lake Baikal. One of the main tasks of data analysis in the TAIGA-HiSCORE experiment is to determine the axis direction of the EASs and their core location. These parameters are used to determine the source of gamma rays and play an important role in estimating the energy of the primary particle. The data collected by HiSCORE stations include signal amplitude and arrival time and allow for estimation of the shower direction of arrival. In this work, we use Monte Carlo simulation data for HiSCORE to demonstrate the feasibility of determining the EAS axis directions with artificial neural networks. Our approach employs multilayer perceptrons with skip connections, which take data from subsets of HiSCORE stations as input. Multiple station subsets are selected to derive more accurate composite estimates. Furthermore, we use a two-stage algorithm, where the initial direction estimates in the first stage are refined in the second stage. The final estimates have an average error of less than 0.25°. We plan to use this approach as a part of multimodal analysis of data obtained from several types of detectors used in the TAIGA experiment.

Keywords: extensive area shower, EAS direction, Cherenkov detector, machine learning, artificial neural network, multilayer perceptron, skip connections

DOI: 10.3103/S0027134924702199

1. INTRODUCTION

High-energy cosmic and gamma rays collide with the nuclei of atmospheric atoms, creating cascades of secondary particles known as extensive air showers (EASs). These showers can be detected and registered using various instruments such as imaging atmospheric Cherenkov telescopes or arrays of Cherenkov detectors of different types. Experimental facilities that employ multiple detector types simultaneously include, for example, TAIGA [1] and LHAASO [2]. The obtained data allow experimenters to determine the direction of the EAS axis, their core location, the type of the primary particle and its energy.

Estimates of the shower axis direction can be obtained from measurements of the shower registration time by several detectors distributed over a large area. This method is used in TAIGA-HiSCORE [3], LHAASO [2], and HAWC [4] experiments. In this paper, we demonstrate the feasibility of inferring the axis direction of the EAS from the HiSCORE array data using fully connected neural networks. We use Monte Carlo-simulated data for EASs produced by gamma rays.

Convolutional neural networks seem to be a natural choice for this problem, since HiSCORE stations form a two-dimensional grid. However, the works [5, 6] using this approach have produced estimates that are less accurate than previously developed methods, such as [7]. We use multilayer skip-connected perceptrons instead. They take data from a fixed number of HiSCORE stations as input and produce partial direction estimates. To use all of the available data, we combine multiple partial estimates based on different subsets of stations to derive composite direction estimates.

*E-mail: kryukov@theory.sinp.msu.ru
**E-mail: s.p.polyakov@gmail.com

To improve the accuracy of direction estimates, we added a second stage of the algorithm using a separate neural network. The initial direction estimates (the composite estimates produced in the first stage) are used to transform the input data for the second stage, where the corrections to the initial estimates are calculated. Same as the first stage, multiple partial corrections calculated by the neural network are combined to derive composite corrections. The final estimates obtained in the second stage are comparable in accuracy to those produced by the traditional approach.

2. METHODS

2.1. Two-Stage Algorithm

We have a two-stage algorithm, with each stage using its own artificial neural network. The first-stage network (ANN-1) computes initial direction estimates, and the second-stage network (ANN-2) refines them. This is achieved by transforming the input data for each event based on the initial direction estimate. The transformation consists of projecting the HiSCORE stations onto a plane orthogonal to the estimated direction and adjusting the signal recording times of the stations. Since the shower is symmetrical about its axis, the adjusted times should have axial symmetry around the intersection of the shower axis and the projection plane. Inaccuracies of initial directions result in deviations from this symmetry that should be easier detected by ANN-2, allowing it to calculate the necessary corrections.

2.2. Partial and Composite Estimates

Each stage of the algorithm uses a neural network that takes data from a fixed number of stations. Any subset of triggered stations (stations recording signal at or above the threshold response amplitude) can be used. The outputs of neural networks thus only use part of the available data for the event. We call them partial direction estimates for ANN-1 and partial corrections for ANN-2. By combining multiple partial estimates (corrections) for the same event based on different subsets of triggered stations, we obtain composite estimates (corrections). The final direction estimates by the algorithm are composite estimates by the first stage with composite corrections by the second stage.

2.3. Input Data

The dataset we use consists of events simulated using the Monte Carlo software for the TAIGA experiment [8, 9]. The primary particles are gamma rays with energies from 100 to 1000 TeV. The range of EAS zenith and azimuth angles is $30° \leq \theta_0 \leq 40°$, $120° \leq \phi_0 \leq 240°$, respectively. The Cherenkov radiation produced by the showers is detected by an array of 121 HiSCORE stations with a threshold response amplitude of 100 photoelectrons. The data from some stations were discarded to ensure that for any event the interval between signal detections by different stations never exceeds 3 μs. Events with fewer than 10 triggered stations were excluded, except for the training set for ANN-1, which was expanded using events with 8 or 9 triggered stations. In the remaining 79 745 events, the average number of triggered stations is about 42. These events were randomly divided into training, validation, and test sets, comprising 66 490, 7447, and 5808 events, respectively.

The input data for the neural networks are obtained from fixed-size subsets of triggered stations. The subset sizes are $K = 8$ for ANN-1 and $K = 10$ for ANN-2. Each input vector includes the station coordinates, the number of detected photoelectrons, and the mean and standard deviation of the detection time for each station in the subset. The stations are sorted by detection time. The shower direction estimates must be shift-invariant, so the detection time and station coordinates are given relative to the first station, resulting in $6K$—4 input values.

We used different algorithms to select station subsets for the training set and for the validation and test sets. For the training set, we aimed to moderately expand the data without introducing excessive redundancy. For the validation and test sets, the accuracy of the composite estimates generally increases with the number of subsets, so we used large numbers of subsets per event.

For the ANN-1 training set, we selected random subsets in a way that ensured that no pair had more than two stations in common. This resulted in 3.88 million training input vectors. For the main validation and test sets, we chose $m = 120$ as the maximum number of subsets per event. In addition, sets with $m = 30$, 60, and 240 were used.

At the second stage, generation of the training data can follow two approaches. The first one is a specialized approach trying to train the neural network to correct the estimation errors made by the first stage neural network ANN-1. The second one does not focus on the specific ANN-1 and is aimed at correcting any estimation errors of the magnitude similar to the errors made by ANN-1. We chose the second approach and randomly generated up to 100 direction estimates for each event with θ and

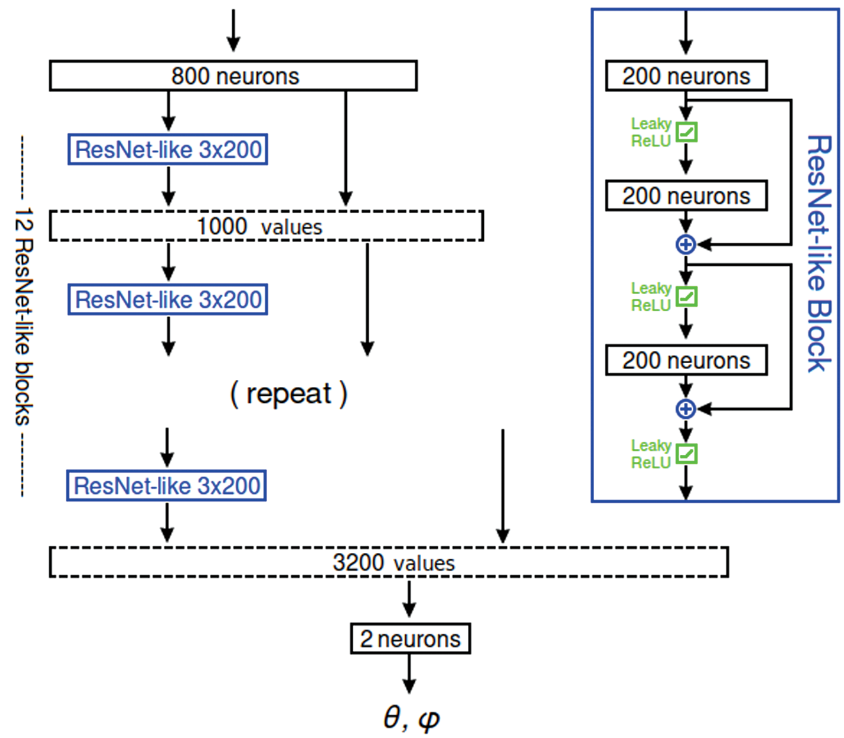

Fig. 1. The architecture of the first stage neural network.

ϕ angles from the normal distributions $\mathcal{N}(\theta_0, 1.5°)$, $\mathcal{N}(\phi_0, 3°)$. Such an approach is equivalent to data augmentation. We chose standard deviations 1.5° and 3° that are approximately 5–6 times larger than the standard deviations of the respective angles of the initial direction estimates to better cover the cases with large errors. For each pair of an event and a direction estimate we independently selected random subsets of triggered stations such that no pair shared more than one station. This resulted in 42.9 million training input vectors. Validation and test sets were generated using composite direction estimates calculated in the first stage. Each has the same maximum number of subsets per event m that was used to derive the corresponding composite estimates.

2.4. Architecture of the Neural Networks

In the architecture of the proposed neural network, we use two types of skip connections: ResNet-like connections using addition and DenseNet-like connections using concatenation [10, 11]. These types of skip connections were proposed for convolutional NNs to mitigate the vanishing gradient problem. We use their analogs for fully connected layers. Smaller blocks with fixed-size layers and residual connections (ResNet-like blocks) produce outputs that are concatenated with the previous outputs to form the inputs for the next block. Figure 1 shows the architecture of ANN-1. The first densely connected layer has 800 neurons, followed by 12 ResNet-like blocks containing 3 layers of 200 neurons with two residual connections. ANN-2 is similar, but with 400 neurons in each layer of its ResNet-like blocks instead of 200. Batch normalization and leaky ReLU activation are applied after each hidden layer.

The output of both neural networks is two linearly activated values, which are interpreted as zenith and azimuth angles θ_1, ϕ_1 for ANN-1 or corrections $\Delta\theta_2$, $\Delta\phi_2$ for ANN-2, in degrees.

2.5. Training

The neural networks were implemented and trained using TensorFlow.

For ANN-1, the loss function we used was $\sin^2\omega_1$ where ω_1 is the angle between the Monte Carlo axis direction and the direction estimate by the neural network. The network was trained for 400 epochs, and the parameter values at epoch 330 were chosen based on the accuracy of the composite estimates for the primary validation set.

For ANN-2, the loss function was

$$(\Delta\theta_2 - \Delta\theta_0)^2 + \sin^2\theta(\Delta\phi_2 - \Delta\phi_0)^2,$$

where $\Delta\theta_0 = \theta - \theta_0$, $\Delta\phi_0 = \phi - \phi_0$ are the corrections that the network needs to learn, and (θ, ϕ) is the direction estimate that was used to transform the input data. The network was trained for 50 epochs,

Table 1. Mean angles between EAS directions and their composite estimates by ANN-1

Weight	Mean	Median
1	0.2802°	0.2654°
S	0.2729°	0.261°
S^2	0.2697°	0.26°
S^3	0.269°	0.2611°

and the parameter values at epoch 45 were chosen. In both cases, Adam optimizer [12] with the learning rate 10^{-4} was used.

3. RESULTS

We used our two-stage algorithm with the trained networks to obtain the EAS axis direction estimates for the validation and test sets. Estimation errors (angles between Monte Carlo EAS axis directions and their estimates) for partial and composite estimates were calculated for each stage. The partial and composite estimation errors are denoted by ω and Ω, respectively.

In the first stage, partial direction estimates produced by ANN-1 for each input vector in the primary test set (with up to $m = 120$ vectors per event) have the mean error $\overline{\omega}_1 = 0.546°$.

The simplest way to derive a composite estimate from partial estimates is to calculate their arithmetic mean. However, these estimates can be improved by giving more weight to the subsets in which the stations recorded higher amplitudes and by using median values for θ and ϕ instead of mean. We compared eight composite estimates using weighted means and weighted medians with weights 1, S, S^2, and S^3, where

$$S = \sum_{k=1}^{K} A_k$$

and A_k is the number of photoelecrons detected by kth station of the subset, $1 \leq k \leq K$. Table 1 shows the mean errors $\overline{\Omega}_1$ of the eight composite estimates for the primary test set. On average, the most accurate composite estimates on the primary validation set were S^2-weighted median estimates, so they were selected as the output for the first stage of the algorithm and the initial estimates used in the second stage data transformation.

For the primary test set, the mean error of the first stage composite direction estimates $\overline{\Omega}_1$ is 0.26°. The distribution of ω_1 and Ω_1 errors is shown in Fig. 2.

Table 2. Mean angles between EAS directions and their composite S^2-weighted median estimates by ANN-1 with composite corrections by ANN-2

Weight	Mean	Median
1	0.2235°	0.2193°
S	0.2196°	0.2165°
S^2	0.2176°	0.2153°
S^3	0.2171°	0.2159°

In the second stage, the composite estimates by ANN-1 with partial corrections by ANN-2 have the mean error $\overline{\omega}_2 = 0.364°$ for the test set.

We compared mean and median composite corrections with weights 1, S, S^2, and S^3 for the primary validation set, and selected the S^2-weighted median correction. Table 2 shows the mean errors $\overline{\Omega}_2$ of the initial estimates with the eight composite corrections for the primary test set.

The final result of the algorithm is the composite estimate produced by the first stage with the composite correction by the second stage. For the primary test set, the final direction estimates have the mean value of estimation errors 0.215°, median 0.125°, RMS 0.344°. The distribution of the ω_2 and Ω_2 errors is shown in Fig. 3.

The final estimates tend to become more accurate with the number of triggered stations: for the 5237 test events with at least 15 triggered stations $\overline{\Omega}_2 = 0.183°$, for the 4670 events with at least 20 triggered stations $\overline{\Omega}_2 = 0.162°$, for the half of the events with at least 38 triggered stations $\overline{\Omega}_2 = 0.116°$, and for the 1341 events with at least 60 triggered stations $\overline{\Omega}_2 = 0.0885°$. Figure 4 shows the mean estimation errors $\overline{\Omega}_2$ depending on the number of triggered stations.

Table 3. The weight formulas used by composite estimates and composite corrections and the corresponding mean estimation errors by the first and the second stages for the test sets with at most m input entries per event. S is the total number of photoelectrons detected by the stations in the subset

m	Stage 1 weight	$\overline{\Omega}_1$	Stage 2 weight	$\overline{\Omega}_2$
30	S	0.2711°	S	0.2222°
60	S	0.2654°	S^2	0.2175°
120	S^2	0.26°	S^2	0.2153°
240	S^3	0.2561°	S^2	0.2135°

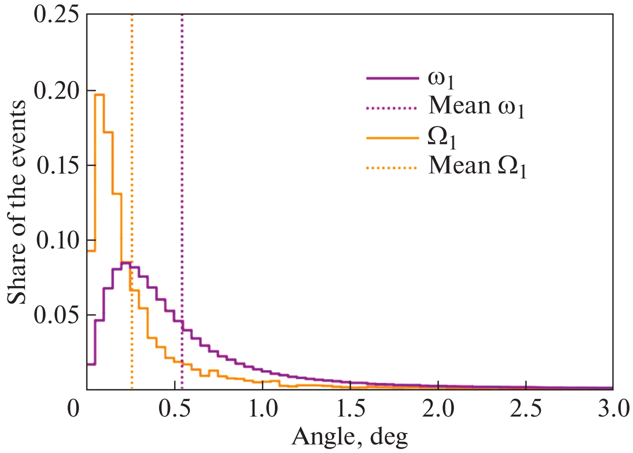

Fig. 2. The distribution of the angles between EAS directions and their partial and composite estimates by the first stage of the algorithm. (The part where the fractions are indistinguishable from zero is not shown; $\max \omega_1 = 15.135°$, $\max \Omega_1 = 4.714°$.)

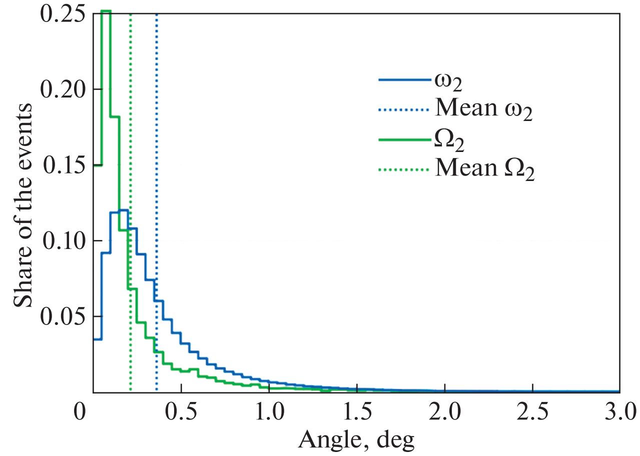

Fig. 3. The distribution of the angles between the EAS direction and its estimates by ANN-2 for the primary test set. (The part where the fractions are indistinguishable from zero is not shown; $\max \omega_2 = 6.312°$, $\max \Omega_2 = 4.544°$.)

Less accurate estimates can be obtained at lower computational cost by decreasing the number of station subsets. Conversely, increasing the number of subsets tends to increase the accuracy of the composite estimates. Table 3 shows the mean errors of the composite estimates obtained from the test sets generated with at most $m = 30$, 60, 120, and 240 station subsets per event. In each case, the corresponding validation set was used to select the most accurate composite estimate. All composite estimates use weighted medians with the weight formulas shown in the table.

The accuracy of the conventional method for estimating EAS directions based on TAIGA HiSCORE data is on the order of 0.1° [7, 13]. When applied to the data that we used, the preliminary results were less accurate: the mean estimation error was 0.349°, median 0.12°, RMS 0.67° [14].

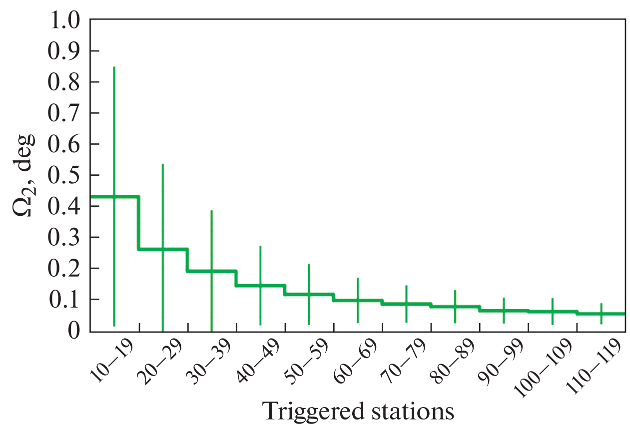

Fig. 4. The mean estimation errors for the test events grouped by the number of triggered stations.

4. CONCLUSIONS

We use multilayer perceptrons with skip connections to obtain EAS direction estimates based on data from subsets of TAIGA-HiSCORE stations. The obtained results are combined to obtain composite estimates. The algorithm consists of two stages: initial axis direction estimate and its refinement.

Our results show that artificial neural networks estimate EAS directions with accuracy comparable to that of conventional methods. For the events of our test set, the average error of the estimate is 0.215°, and if we consider only the events detected by at least 60 of the 121 stations, the average error is 0.0885°.

The TAIGA installation includes several types of detectors located in the same place as HiSCORE. We plan to integrate the proposed approach for the analysis of multimodal data, which will include data from different setups.

ACKNOWLEDGMENTS

The authors would like to thank the TAIGA collaboration for support and data provision. The work was carried out using equipment provided by the MSU Development Program.

FUNDING

This study was supported by the Russian Science Foundation, grant no. 24-11-00136.

CONFLICT OF INTEREST

The authors of this work declare that they have no conflicts of interest.

REFERENCES

1. N. Budnev, I. Astapov, P. Bezyazeekov, E. Bonvech, A. Borodin, A. Bulan, A. Chiavassa, D. Chernov, A. Dyachok, A. Gafarov, A. Garmash, V. Grebenyuk, O. Gress, E. Gress, T. Gress, A. Grinyuk, O. Grishin, A. D. Ivanova, A. L. Ivanova, N. Kalmykov, V. Kindin, S. Kiryuhin, R. Kokoulin, K. Komponiets, E. Korosteleva, V. Kozhin, E. Kravchenko, A. Kryukov, L. Kuzmichev, A. Lagutin, M. Lavrova, Y. Lemeshev, B. Lubsandorzhiev, N. Lubsandorzhiev, A. Lukanov, D. Lukyantsev, S. Malakhov, R. Mirgazov, R. Monkhoev, E. Okuneva, E. Osipova, A. Pakhorukov, et al. (TAIGA Collaboration), Nucl. Instrum. Methods Phys. Res., Sect. A **1039**, 167047 (2022).
https://doi.org/10.1016/j.nima.2022.167047
2. Zh. Cao, D. della Volpe, S. Liu, X. Bi, Ya. Chen, B. D. Piazzoli, L. Feng, H. Jia, Zh. Li, X. Ma, X. Wang, X. Zhang, E. Referees, :, X. Qie, H. Hu, I. Referees, :, A. Sáiz, R. Yang, A. Addazi, K. Belotsky, V. Beylin, Y.-J. Bi, M.-J. Che, S.-Z. Chen, Y.-D. Cheng, A. Chiavassa, M. Cirelli, G. D. Sciascio, A. Esmaili, K. Fang, N. Fornengo, Q. Gou, Y.-Q. Guo, Q. Gan, G.-H. Gong, M.-H. Gu, H. He, H.-H. He, Ch. Hou, X.-T. Huang, W.-H. Huang, M. Kachekriess, M. Khlopov, V. Korchagin, A. Korochkin, et al., Chin. Phys. C **46**, 035001 (2022).
https://doi.org/10.48550/arXiv.1905.02773
3. O. Gress, I. Astapov, N. Budnev, P. Bezyazeekov, A. Bogdanov, V. Boreyko, M. Brückner, A. Chiavassa, O. Chvalaev, A. Dyachok, T. Gress, S. Epimakhov, E. Fedoseev, A. Gafarov, N. Gorbunov, V. Grebenyuk, A. Grinuk, O. Grishin, D. Horns, A. Ivanova, A. Kalinin, N. Karpov, N. Kalmykov, Yu. Kazarina, N. Kirichkov, S. Kiryuhin, R. Kokoulin, K. Komponiest, E. Korosteleva, V. Kozhin, M. Kunnas, L. Kuzmichev, V. Lenok, B. Lubsandorzhiev, N. Lubsandorzhiev, R. Mirgazov, R. Mirzoyan, R. Monkhoev, et al. (TAIGA Collaboration), Nucl. Instrum. Methods Phys. Res., Sect. A **845**, 367 (2017).
https://doi.org/10.1016/j.nima.2016.08.031
4. A. U. Abeysekara, A. Albert, R. Alfaro, C. Alvarez, J. D. Álvarez, M. Araya, J. C. Arteaga-Velázquez, K. P. Arunbabu, D. A. Rojas, H. A. A. Solares, R. Babu, A. S. Barber, A. Becerril, E. Belmont-Moreno, S. Y. Benzvi, O. Blanco, J. Braun, C. Brisbois, K. S. Caballero-Mora, J. I. C. Martínez, T. Capistrán, A. Carramiñana, S. Casanova, M. Castillo, O. Chaparro-Amaro, U. Cotti, J. Cotzomi, S. C. De León, E. De La Fuente, C. De León, T. De Young, R. D. Hernandez, B. L. Dingus, M. A. Duvernois, M. Durocher, J. C. Díaz-Vélez, R. W. Ellsworth, K. Engel, C. Espinoza, K. L. Fan, K. Fang, B. Fick, H. Fleischhack, J. L. Flores, N. Fraija, J. A. García-González, G. Garcia-Torales, et al., Nucl. Instrum. Methods Phys. Res., Sect. A **1052**, 168253 (2023).
https://doi.org/10.1016/j.nima.2023.168253
5. A. A. Vlaskina and A. Kryukov, in *Proceedings of The 6th International Workshop on Deep Learning in Computational Physics—PoS(DLCP2022)* (Sissa Medialab, 2022), Vol. 429, p. 6.
https://doi.org/10.22323/1.429.0006
6. A. P. Kryukov, A. A. Vlaskina, S. P. Polyakov, E. O. Gres, A. P. Demichev, Yu. Yu. Dubenskaya, and D. P. Zhurov, Moscow Univ. Phys. Bull. **78** (S1), S32 (2023).
https://doi.org/10.3103/s0027134923070172
7. M. Tluczykont, I. I. Astapov, A. K. Awad, P. A. Bezyazeekov, M. Blank, E. A. Bonvech, A. N. Borodin, A. V. Bulan, M. Brückner, N. M. Budnev, A. Chiavassa, D. V. Chernov, A. N. Dyachok, A. R. Gafarov, A. Yu. Garmash, V. M. Grebenyuk, O. A. Gress, E. Gress, T. I. Gress, O. G. Grishin, A. A. Grinyuk, D. Horns, A. L. Ivanova, N. N. Kalmykov, V. V. Kindin, S. N. Kiryuhin, R. P. Kokoulin, K. G. Kompaniets, E. E. Korosteleva, V. A. Kozhin, E. A. Kravchenko, A. P. Kryukov, L. A. Kuzmichev, A. A. Lagutin, M. Lavrova, Yu. E. Lemeshev, B. K. Lubsandorzhiev, N. B. Lubsandorzhiev, A. D. Lukanov, D. S. Lukyantsev, R. R. Mirgazov, R. Mirzoyan, R. D. Monkhoev, E. A. Osipova, A. L. Pakhorukov, A. Pan, L. A. Panasenko, L. V. Pankov, A. D. Panov, A. A. Petrukhin, D. A. Podgrudkov, V. A. Poleschuk, E. G. Popova, et al. (TAIGA Collaboration), Phys. At. Nucl. **84**, 1045 (2021).
https://doi.org/10.1134/s1063778821130378
8. E. B. Postnikov, I. I. Astapov, P. A. Bezyazeekov, V. F. Boreyko, A. N. Borodin, M. Brueckner, N. M. Budnev, A. Chiavassa, A. N. Dyachok, O. L. Fedorov, A. R. Gafarov, A. Yu. Garmash, N. V. Gorbunov, V. M. Grebenyuk, O. A. Gress, T. I. Gress, O. G. Grishin, A. A. Grinyuk, D. Horns, A. L. Ivanova, N. N. Kalmykov, Y. A. Kazarina, V. V. Kindin, S. N. Kiryuhin, P. S. Kirilenko, R. P. Kokoulin, K. G. Kompaniets, E. E. Korosteleva, V. A. Kozhin, E. A. Kravchenko, M. Kunnas, A. A. Lagutin, L. A. Kuzmichev, Yu. Lemeshev, V. V. Lenok, B. K. Lubsandorzhiev, N. B. Lubsandorzhiev, R. R. Mirgazov, R. Mirzoyan, R. D. Monkhoev, E. A. Osipova, A. L. Pakhorukov, M. I. Panasyuk, L. V. Pankov, A. A. Petrukhin, V. A. Poleschuk, M. Popescu, E. G. Popova, A. Porelli, E. B. Postnikov, V. V. Prosin, V. S. Ptuskin, E. V. Rjabov, G. I. Rubtsov, A. A. Pushnin, R. I. Raikin, Y. I. Sagan, B. M. Sabirov, V. S. Samoliga, Yu. A. Semeney, A. A. Silaev, A. A. Silaev, A. Yu. Sidorenkov, A. V. Skurikhin, et al. (TAIGA Collaboration), Bull. Russ. Acad. Sci.: Phys. **83**, 955 (2019).
https://doi.org/10.3103/s1062873819080331
9. A. Grinyuk, E. Postnikov, and L. Sveshnikova, Phys. At. Nucl. **83**, 262 (2020).
https://doi.org/10.1134/s106377882002012x
10. K. He, X. Zhang, S. Ren, and J. Sun, in *Computer Vision—ECCV 2016*, Ed. by B. Leibe, J. Matas,

N. Sebe, and M. Welling, Lecture Notes in Computer Science, Vol. 9908 (Springer, Cham, 2016), p. 630. https://doi.org/10.1007/978-3-319-46493-0_38

11. G. Huang, Zh. Liu, L. Van Der Maaten, and K. Q. Weinberger, in *2017 IEEE Conference on Computer Vision and Pattern Recognition (CVPR), Honolulu, HI, 2017* (IEEE, 2017), p. 2261. https://doi.org/10.1109/cvpr.2017.243
12. D. P. Kingma and J. Ba, arXiv Preprint (2014). https://doi.org/10.48550/arXiv.1412.6980
13. M. Tluczykont, O. Gress, E. Korosteleva, L. Kuzmichev, A. Pakhorukov, A. Porelli, V. Prosin, L. Sveshnikova, R. Wischnewski, I. Astapov, P. Bezyazeekov, V. Boreyko, A. Borodin, M. Brueckner, N. M. Budnev, A. Chiavassa, A. N. Dyachok, O. Fedorov, A. Gafarov, A. Garmash, N. Gorbunov, V. Grebenyuk, T. I. Gress, O. Grishin, A. Grinyuk, D. Horns, A. Ivanova, N. Kalmykov, Y. Kazarina, V. Kindin, P. Kirilenko, S. Kiryuhin, R. Kokoulin, K. Kompaniets, V. V. Kozhin, E. Kravchenko, M. Kunnas, Y. Lemeshev, V. Lenok, B. Lubsandorzhiev, N. Lubsandorzhiev, R. Mirgazov, R. Mirzoyan, R. Monkhoev, R. Nachtigall, E. Osipova, M. I. Panasyuk, L. Pankov, A. Petrukhin, V. Poleschuk, E. Popescu, E. Popova, et al. (TAIGA Collaboration), in *Proceedings of 35th International Cosmic Ray Conference—PoS(ICRC2017)* (Sissa Medialab, 2017), Vol. 2017, p. 759. https://doi.org/10.22323/1.301.0759
14. E. A. Osipova, personal communication (2024).